Molecular Therapy
Nucleic Acids
Original Article

ceRNA regulatory network of FIH inhibitor as a radioprotector for gastrointestinal toxicity by activating the HIF-1 pathway

Yu-wei Yang,[1,2] Xin Meng,[1,2] Yuan-yuan Meng,[1,2] Hai-kang Tang,[1] Ming-hui Cheng,[1] Zi-qi Zhang,[1] Wen-qing Xu,[1] and Wei Long[1]

[1]Tianjin Key Laboratory of Radiation Medicine and Molecular Nuclear Medicine, Institute of Radiation Medicine, Chinese Academy of Medical Science and Peking Union Medical College, Tianjin 300192, China

Given the relentless renewal ability of intestinal crypt-base stem cells, small intestine in the gastrointestinal (GI) tract is more vulnerable to radiation-induced disruption. Through promoting epithelial integrity and reducing intracellular reactive oxygen species (ROS) levels, hypoxia-inducible factors (HIFs) have been proved to exhibit radioprotective effects in the GI tract. Therefore, enhancing stability or transcriptional activity of HIFs might be a therapeutic strategy for developing radioprotectors. Factor inhibiting HIF (FIH or HIF-1AN) can hamper transcriptional capacity of HIF-1α via interacting with Asn803 in its C-terminal domain. Previously, we discovered promoting HIF-1α transcriptional activity *in vitro* by FIH inhibitor-N-oxalyl-D-phenylalanine (NOFD) exerts radioprotection on cells. However, the radioprotective effect of FIH inhibitor on the GI tract and its competing endogenous RNA (ceRNA) regulatory network from the FIH/HIF axis has never been addressed. Here we verified radioprotection of NOFD for the GI tract by an animal model and performed whole-transcriptome analysis to fully elucidate the radioprotective mechanism from the FIH/HIF axis against GI syndrome. We identified two novel circular RNAs (circRNAs) (circRNA_2909 and circRNA_0323) and two long non-coding RNAs (lncRNAs) (NONMMUT140549.1 and NONMMUT148249.1) that promote expression of *HIF1A* and *NOS2* in the HIF-1 pathway by sponging microRNAs (miRNAs), especially mmu-miR-92a-1-5p. The de-repression of HIF-1α transcriptional capacity by inhibiting FIH proteomic activity suggests a new therapeutic strategy in alleviating radiation-induced GI syndrome.

INTRODUCTION

During nuclear accidents or terrorism, radiation doses exceeding 10 Gy will immediately cause gastrointestinal (GI) damage and bone marrow failure.[1,2] This transient exposure to a large dose of ionizing radiation (IR) extremely affects the survival of victims. Radiation-induced severe bone marrow depression can be rescued by bone marrow transplantation or intravenous hematopoietic growth factors, while ideal mitigators in modulating radiation-induced GI toxicity are still deficient.[3–5] Previous studies demonstrated that hypoxia-inducible factors (HIFs), which are the key regulators in response to an oxygen-deficient condition, can be a therapeutic target for radiation-induced GI syndrome (RIGS) by promoting epithelial integrity and regulating immune cell functions.[6–8] Additionally, through facilitating anaerobic metabolism, HIF-1α reduces intracellular reactive oxygen species (ROS) levels by inhibiting their production.[9] This conclusion corresponds to the result obtained from our former study, in which accelerated transcriptional activity of HIF-1α alleviates IR-induced DNA damage and cellular apoptosis via diminishing ROS levels.[10] Accordingly, enhancing HIF-1α activity has recently been considered as a new strategy for developing radioprotectors.

The intercellular activity of HIF complex is synergistically modulated by two oxygen sensors: prolyl hydroxylases (PHDs 1-3) and factor inhibiting HIF (FIH or HIF-1AN).[11] PHDs determine HIF stability by hydroxylating proline residues on HIF-α subunits, while FIH regulates its transcriptional capacity via interacting with Asn803 in the C-terminal domain (C-TAD) of the HIF-1α.[12–14] As FIH possesses higher oxygen affinity than PHDs, it still retains active enzymatic activity at lower oxygen conditions, such as the GI tract.[15–17] Therefore, apart from stabilizing the HIF complex via blocking PHDs,[8,18] FIH inhibitors can be another mainstream strategy in developing radioprotectors (especially for GI) through promoting HIF-1α transcriptional activity.

We demonstrated previously that selective inhibition of FIH by N-oxalyl-D-phenylalanine (NOFD) exhibits radioprotection on cells by reducing intracellular ROS levels, hampering DNA damage

Received 16 March 2021; accepted 13 May 2021;
https://doi.org/10.1016/j.omtn.2021.05.008.

[2]These authors contributed equally

Correspondence: Wen-qing Xu, Tianjin Key Laboratory of Radiation Medicine and Molecular Nuclear Medicine, Institute of Radiation Medicine, Chinese Academy of Medical Science and Peking Union Medical College, Tianjin 300192, China.
E-mail: xuwenqing@irm-cams.ac.cn
Correspondence: Wei Long, Tianjin Key Laboratory of Radiation Medicine and Molecular Nuclear Medicine, Institute of Radiation Medicine, Chinese Academy of Medical Science and Peking Union Medical College, Tianjin 300192, China.
E-mail: longwei@irm-cams.ac.cn

and apoptosis, as well as significantly increasing the transcriptional level of downstream genes regulated by HIF-1α.[10] In this study, we used a C57BL/6 mouse model of radiation-induced small intestinal toxicity to further investigate its radioprotection of the GI tract first. Moreover, to elucidate the underlying mechanism of the FIH/HIF axis in IR-induced GI syndrome, we performed whole-transcriptome analysis in control and NOFD pre-treatment groups and obtained their competing endogenous RNA (ceRNA) regulatory network.

The ceRNA hypothesis indicates a novel transcriptional regulatory network, which was first demonstrated by Salmena et al.[19] in 2011. Among this intricate RNA crosstalk, diverse RNA transcripts, including mRNAs, long non-coding RNAs (lncRNAs), circular RNAs (circRNAs), and pseudogenes, will co-regulate each other via competitively binding to shared microRNAs (miRNAs).[20]

In this study, we utilized a deep RNA sequencing method to obtain differentially expressed transcripts against radiation-induced GI toxicity mouse models in NOFD or isotonic saline pre-treatment groups. After the construction of lncRNA/circRNA-associated ceRNA networks, we identified 4 crucial hub genes, namely *EGFR*, *HIF1A*, *NOS2*, and *CDKN1A*, in this intricate RNA crosstalk. Additionally, two novel circRNAs (circRNA_2909 and circRNA_0323) and two lncRNAs (NONMMUT140549.1 and NONMMUT148249.1) were identified as important upstream regulators in the ceRNA networks of obtained hub genes. Combining all these results, we illustrate the ceRNA regulatory network associated with the FIH/HIF axis for the first time and propose that FIH inhibitors such as NOFD might be a therapeutic strategy in GI radioprotection.

RESULTS

FIH inhibitor-NOFD ameliorates intestine structural injuries induced by 13 Gy ABI

Through referencing the synthetic route in our previous study,[10] we successfully synthesized NOFD (Figure 1A) and obtained its 1H-nuclear magnetic resonance (NMR) (Figure S1) and 13C-NMR spectra (Figure S2). In order to explore the intestinal protective effect of NOFD *in vivo*, the survival rate and body weight against mice were observed after 13 Gy abdominal irradiation (ABI) within 30 days. C57BL/6 mice were injected with NOFD or saline at the indicated time point (Figure 1B). Although there was no death in mice after receiving 13 Gy ABI, NOFD showed a certain protective effect on body weight, especially on the fourth day after irradiation, compared with IR group (Figure 1C). To examine the protective effects of NOFD on radiation-induced GI injuries, we compared the colon length from irradiated male mice with or without NOFD administration. As expected, NOFD replenishment reversed shortening of the colon (Figures 1D and 1E). We further compared the histological manifestations within the small intestines of NOFD-treated or untreated mice post 13 Gy ABI (Figure 1F). At 3.5 days post-irradiation, mucosal architecture destruction, including villous denudation and crypt atrophy, was observed in the IR group, whereas the crypt-villi structures of the small intestine were preserved in NOFD pre-treated mice (IR+NOFD group). The staining of villi+ (Figure 1G), which are intestinal epithelial cells, in small intestinal sections also proved previous results, with significantly higher amounts of villi+ cells in control and IR+NOFD groups compared to the IR group. Furthermore, the crypts and villus heights per circumference were measured as shown in Figures 1H and 1I. All these results demonstrated that NOFD can alleviate the rupture of small intestinal villi and crypt injury caused by high-dose local irradiation.

NOFD improves cell proliferation, reduces cell apoptosis, and enhances epithelial integrity in intestinal crypts after 13 Gy ABI

Intestinal stem cells that express Lgr5+ are reported to facilitate regeneration after radiation-induced damage.[21] To investigate whether NOFD can improve the proliferation of mouse intestinal crypt cells after 13 Gy ABI, we used immunohistochemical staining to detect the number of Lgr5+ cells in the small intestinal crypts. As shown in Figures 2A and 2C, compared with the control group, the number of Lgr5+ intestinal stem cells in the IR group was significantly lower. Similarly, the number of Ki67+ of NOFD-treated mice (IR+NOFD) was observably higher than the IR-only mice (Figures 2B and 2D).

Furthermore, terminal deoxynucleotidyl transferase dUTP nick-end labeling (TUNEL) assay and immunofluorescence analysis were performed to examine cell death of crypt epithelial cells in the small intestine at 3.5 days post ABI. As presented in Figures 2E and 2H, the number of TUNEL-positive cells per field in the IR+NOFD group was significantly lower than irradiated mice treated with saline (IR group). To further validate this conclusion, we analyzed the rate of apoptosis in small intestinal sections of each group post 13 Gy ABI by immunofluorescence staining with caspase-8 and caspase-9 antibodies (Figures 2F and 2G). At 3.5 days after 13 Gy ABI, stained intestinal sections in the IR+NOFD group showed a significantly lower number of apoptotic cells than the IR group (Figures 2I and 2J). These results indicated that hampering FIH activity by NOFD can accelerate the regenerative response of IR-induced intestinal injury and reduce apoptosis in crypts of the intestine.

The pathophysiological mechanism of radiation-induced GI syndrome is closely related to the loss of upper GI integrity, which can lead to fluid loss, unfettered diarrhea and electrolyte imbalance, and, finally, death.[22] We used fluorescein isothiocyanate (FITC)-dextran assay to investigate the integrity of the GI epithelium. After 4 h of gavage, the level of FITC-dextran in the blood was measured. The uptake of FITC-dextran in the blood of the IR+NOFD group decreased by 30% compared to the IR group (Figure 2K). We further validated the upregulated expression of intestinal trefoil factor (*TFF3*/*ITF1*) and multidrug resistance protein 1 (*MDR1*), which is critical to maintaining epithelial integrity after toxic stimuli (Figure 2L), in the IR+NOFD group compared to saline-treated mice post IR. These data suggested that NOFD can effectively maintain intestinal barrier function and intestinal epithelial integrity after 13 Gy ABI.

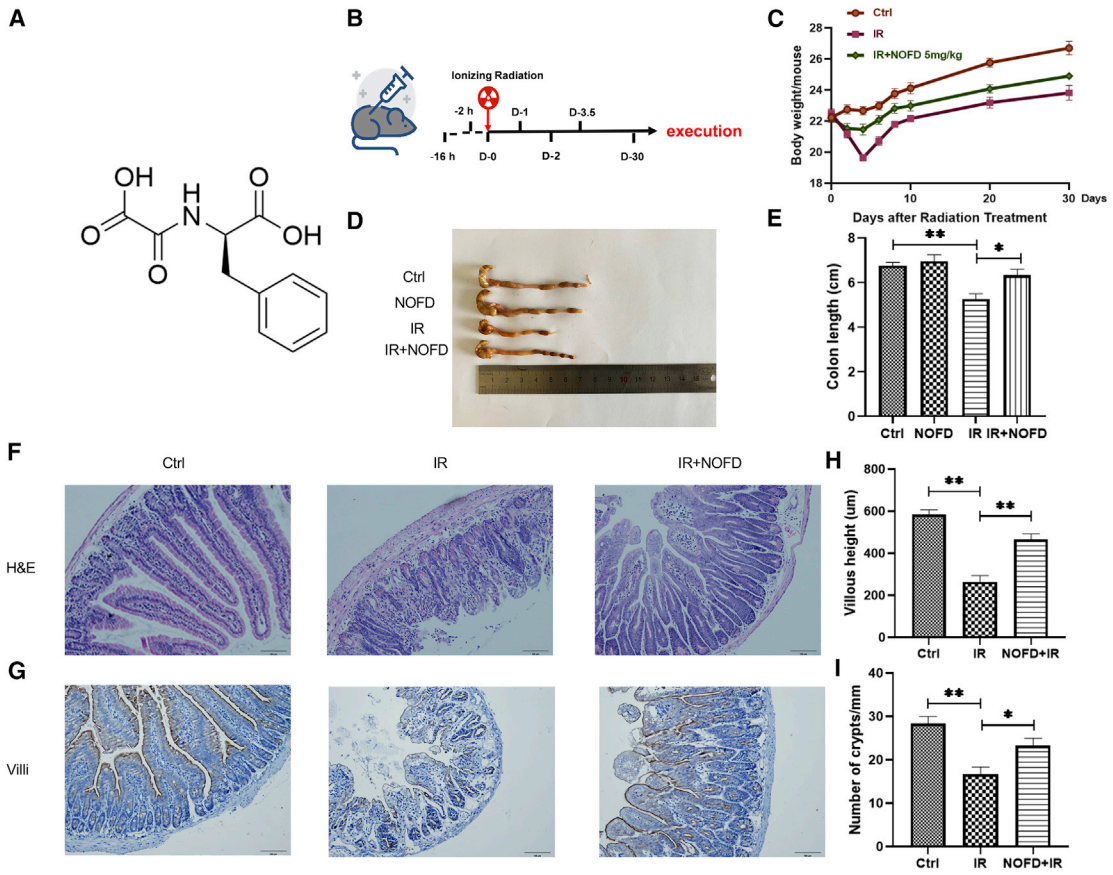

Figure 1. NOFD promotes intestinal structural repair in mice after receiving 13 Gy ABI

(A) Chemical structure of N-oxalyl-D-phenylalanine (NOFD). (B) Mice in the IR+NOFD group received intraperitoneal administration of NOFD (5 mg/kg body weight) as illustrated in the diagram. Mice in the IR group received saline at the same frequency as the IR+NOFD group. Small intestinal segments were collected from the sham-irradiated mice and ABI-exposed mice treated with NOFD/saline 3.5 days after 13 Gy ABI. (C) Body weights of sham-irradiated mice (control), irradiated mice treated with NOFD (IR+NOFD)/saline (IR) in indicated time points before and after 13 Gy ABI. (D and E) Colon tissues and length of mice in control, NOFD, IR, and IR+NOFD groups 4 days after 13 Gy ABI, n = 3 per group. (F) Representative images showing the structure in cross-sections of the small intestine with hematoxylin and eosin (H&E) staining. Scale bar: 100 μm. (G) Immunohistochemistry images showing the expression of villi. Scale bar: 50 μm. (H and I) Histogram showing the number of crypts and villus length in intestinal section from the control group, IR group, and IR+NOFD group. The results are represented as mean ± SEM, n = 6 mice per group. $^{**}p < 0.01$, $^{*}p < 0.05$ by one-way analysis of variance (ANOVA).

Differential expression analyses of all transcripts: IR-NOFD versus IR

To further elucidate the radioprotective mechanism on the FIH/HIF axis, a whole-transcriptome analysis was constructed on radiation-induced GI toxicity mouse models pre-treatment with NOFD. After characterizing RNA transcripts among NOFD or isotonic saline pre-treated groups, we obtained 81.20 G Clean Data (Table S1). All clean reads were aligned to our reference genome, and total mapped reads of 93.28%–97.72% were finally assessed, with 128 lncRNAs and 1,901 circRNAs first identified in this study.

We then analyzed differential expression of these transcripts in three replicates of NOFD pre-treated groups (IR-NOFD) compared to isotonic saline (IR) treatment using DESeq. Cluster analyses of these transcripts were conducted, and the differentially expressed genes (DEGs) (p value < 0.05, $|\lg_2$ fold change (FC)$|$ > 1) were collected as shown in heatmaps (Figure 3); DE-mRNAs (Figure 3A), lncRNAs (Figure 3B), circRNAs (Figure 3C), and miRNAs (Figure 3D) were 2,849, 1,072, 12, and 37, respectively. The upregulated and downregulated DEGs in NOFD pre-treated groups compared with isotonic saline are displayed in Table S2. All these results were further used to construct lncRNA/circRNA-associated ceRNA networks.

Construction of lncRNA/circRNA-associated ceRNA networks

To improve final prediction accuracy, we combined two analytical strategies: (1) base pairing between the seed region of miRNA (conserved 8-mer and 7-mer sites) and sequence of target genes, and (2) expression profiles among them. The extensively used miRNA target predictor miRanda[23] was first adopted to find their

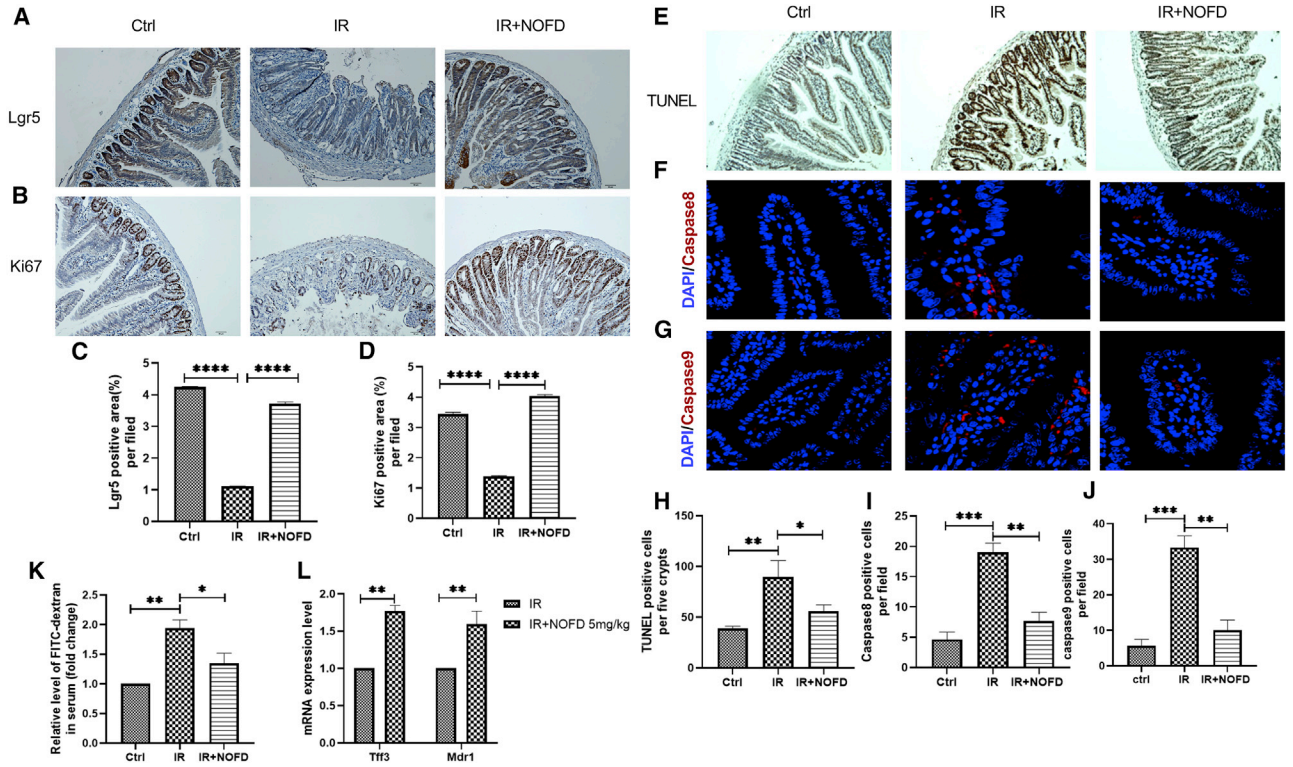

Figure 2. NOFD improves cell proliferation, reduces cell apoptosis, and enhances epithelial integrity in intestinal crypts after 13 Gy ABI

The sections of small intestine were analyzed by immunohistochemical methods. Representative immunostaining images showing the expression of Lgr5+ (A) and Ki67 (B) of the control group, IR group, and IR+NOFD group. Scale bar: 50 μm, n = 6 mice per group. (C and D) Proportional quantization histogram of Lgr5+ and Ki67-positive area in each field. (E) Apoptosis was assayed by terminal deoxynucleotidyl transferase dUTP nick end labeling (TUNEL). Scale bar: 50 μm. (F and G) Representative 4′,6-diamidino-2-phenylindole (DAPI) and caspase 8 and caspase 9-staining images of the small intestine (apoptotic cells stained by caspase 8 and caspase 9 indicated in red, while nuclei were stained by DAPI in blue). Scale bar: 10 μm, n = 6 mice per group. (H) Proportional quantization histogram of TUNEL-positive area in each field. Caspase 8-positive cells (I) and caspase 9-positive cells (J) in a single field of view were quantified. (K) The FITC-dextran in blood serum of mice in the three different groups was assessed at 4 days after 13 Gy ABI. (L) Relative mRNA levels of epithelial barrier genes including *TFF3* and *MDR1* were evaluated in the intestine of IR and IR+NOFD groups. The results are represented as mean ± SEM, n = 3 per group. *p < 0.05, **p < 0.01, ***p < 0.001, ****p < 0.0001 by Student's t test analysis and one-way ANOVA, respectively.

genomic targets through base sequence. Furthermore, correlation analysis was performed to evaluate their expression patterns with parameters including Pearson's $r > 0.7$ and p value < 0.05. We finally obtained 8,742 miRNA-mRNA, 1,419 miRNA-lncRNA, and 20 miRNA-circRNA pairs with high prediction accuracy (Figures 4A–4C). Due to predicted miRNA-target gene pairs, lncRNA/circRNA-miRNA-mRNA networks were further constructed with shared miRNAs ≥ 5 and p value < 0.05. As shown in Figures 4D and 4E, numerous genes were involved in lncRNA/circRNA-associated ceRNA networks disturbing the identification of key regulators. Therefore, we adopted several strategies in the next step to discover hub genes in the ceRNA network correlated with NOFD treatment.

Hub gene identification

Hub genes refer to those genes with high correlation in their regulatory network.[24] Given this feature, a tiny change of their expression may cause immense conversion in whole-gene regulatory modules. Therefore, identifying these key regulators in a tremendous dataset facilitates understanding functional mechanisms of drugs more accurately. As shown in Figure 5, we combined 5 strategies to discover 4 hub genes in IR-NOFD compared to IR groups. With indicated parameters (FC > 2, p < 0.05), 1,425 differentially expressed mRNAs (DE-mRNAs) were separated from all DEGs. Combining 1,312 DE-mRNAs in ceRNA networks, we first obtained 469 intersected DE-mRNAs. Meanwhile, 1,425 DE-mRNAs were analyzed in STRING 11.0 (https://string-db.org/) to construct a protein interaction network (PPI network) among those genes (Figure S3). Two crucial plug-ins, involving MCODE and cytoHubba, were adopted to further refine results after visualizing the PPT network in Cytoscape (v.3.6.0) software. This procedure facilitated our focus on 33 DE-mRNAs. Their expression patterns in each group were visualized in a heatmap (Figure 5A). Several hub genes, including *B4GALT1*, *LMC2*, *CDKN1A*, *CEACAM1*, *FOS*, *APOP*, and *HIF1A*, were extraordinary highly expressed in IR-NOFD groups. Gene Ontology (GO) enrichment (Figure 5B) and Kyoto Encyclopedia of Genes and Genomes (KEGG) pathway analyses among 33 DE-mRNAs were also performed to better understand the functions of those genes.

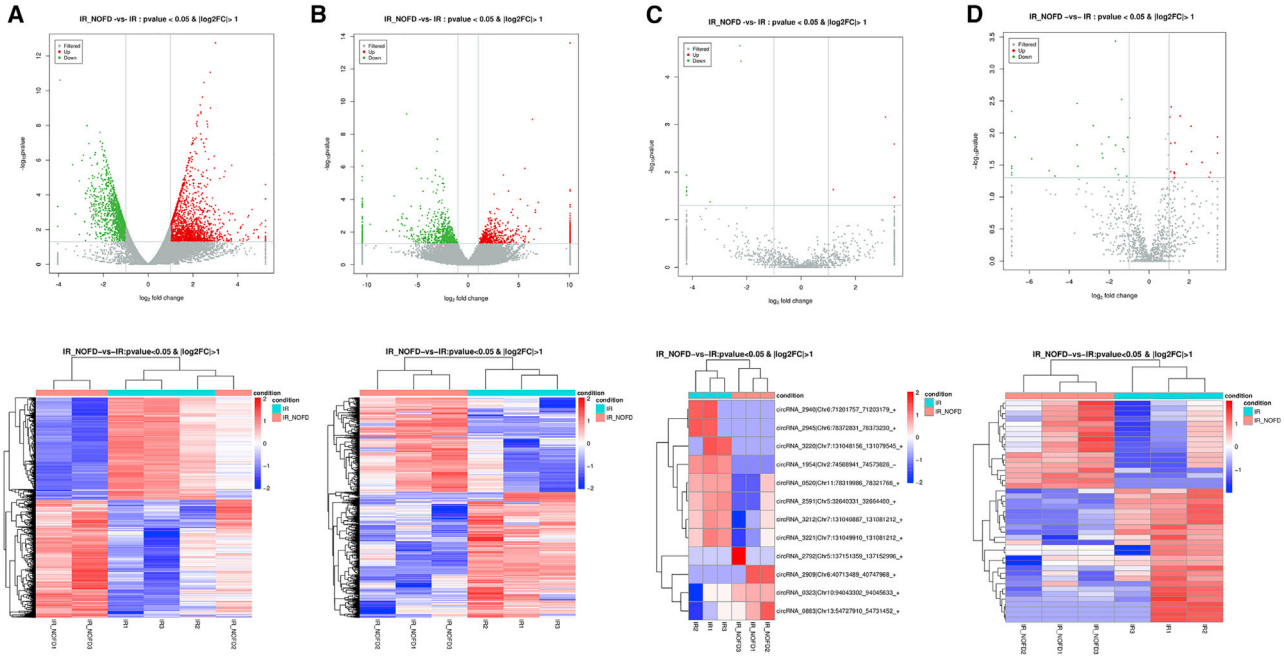

Figure 3. Identification of DEGs between NOFD and isotonic saline pre-treatment groups via deep-sequencing method
Expression profiles for mRNAs (A), lncRNAs (B), circRNAs (C), and miRNAs (D) are visualized in volcano plots and heatmaps.

The top 20 KEGG pathways are displayed in Figure 5C among 33 DE-mRNAs. Considering the inhibition role of NOFD on FIH, we proved that it possesses radioprotective activity mainly through promoting transcriptional activity of the HIF-1α protein after impeding the FIH enzyme.[10] Consequently, we intersected 33 filtrated hub genes with 101 genes in the HIF-1 KEGG pathway and finally obtained 4 genes in this process. They were *EGFR*, *HIF1A*, *NOS2*, and *CDKN1A* (Figure 5; Figure S4).

Construction of 4 hub-gene-associated ceRNA networks

Four hub-gene-associated ceRNA networks are displayed in Figure 6. In circRNA-miRNA-mRNA (Figure 6A), only *HIF1A* and *NOS2* were involved in this network regulated by two novel circRNAs including circRNA_2909|Chr6:40713489_40747968_+ (circRNA2909) and circRNA_0323|Chr10:94043302_94045633_+ (circRNA0323) through competing the miRNA response elements (MREs) on 6 different miRNAs. By combining two analytical plug-ins of MCODE and cytoHubba in Cytoscape, mmu-miR-148a-3p and mmu-miR-92a-1-5p were identified as central nodes in this regulatory network. Compared to the concise results in circRNA-miRNA-mRNA, 4 hub-gene-associated lncRNA networks displayed more intricately. As shown in Figure 6B, NONMMUT140549.1 and NONMMUT148249.1 were eventually filtrated in several lncRNAs as core regulators to influence *HIF1A* and *NOS2* expression through mmu-miR-20a-5p, mmu-miR-92a-1-5p, and mmu-miR-1983. After we identified crucial transcripts in ceRNA networks, we decided to verify their expressional association through evaluating circRNA/lncRNA-mRNA Pearson correlation coefficients. In total, determined circRNAs and lncRNAs were highly consistently expressed with *HIF1A* and *NOS2* followed by Pearson's $r > 0.6$ (Figures 6C and 6D). Their expression values are indicated in Table S3.

Validation

In a previous study, NOFD is a selective inhibitor for FIH.[25] To confirm its suppressing role on FIH, we analyzed asparaginyl hydroxylation activity of FIH on HIF-1α C-TAD transcriptional domain. Through evaluating a set of hypoxic genes related to C-TAD of HIF-1α,[26] we confirmed that *HK2*, adrenomedullin (*ADM*), *VEGFA*, and *SLC2A1* were upregulated in NOFD pre-treatment groups without extraordinary change in FIH expression (Figures 7A and 7G). This result was coincident with RNA sequencing (RNA-seq) analysis, which indicates the impeded enzymatic activity of FIH by NOFD. In addition, we successfully validated the upregulated expressions of *HIF1A*, *NOS2*, *EGFR*, and *CDKN1A* in IR-NOFD compared to IR groups by quantitative real-time PCR (Figure 7B) and western blot analyses (Figures 7H and 7I) with another six upregulated and six downregulated mRNAs to prove the accuracy of RNA-seq results (Figure S5). To determined lncRNAs and circRNAs, specific primers were designed to verify their upregulated expression trends (Figures 7C and 7E). However, unspecific transcripts easily contaminate circRNA products due to sequence similarity between back-splice site regions of circRNA and other linear RNAs. Given the high stability of circularized RNA compared to linear RNA, we treated total RNA with RNase R in order to digest all linear RNAs. As shown in Figure 7D, 18S and 28S bands were lost in the RNase-R-treated group,

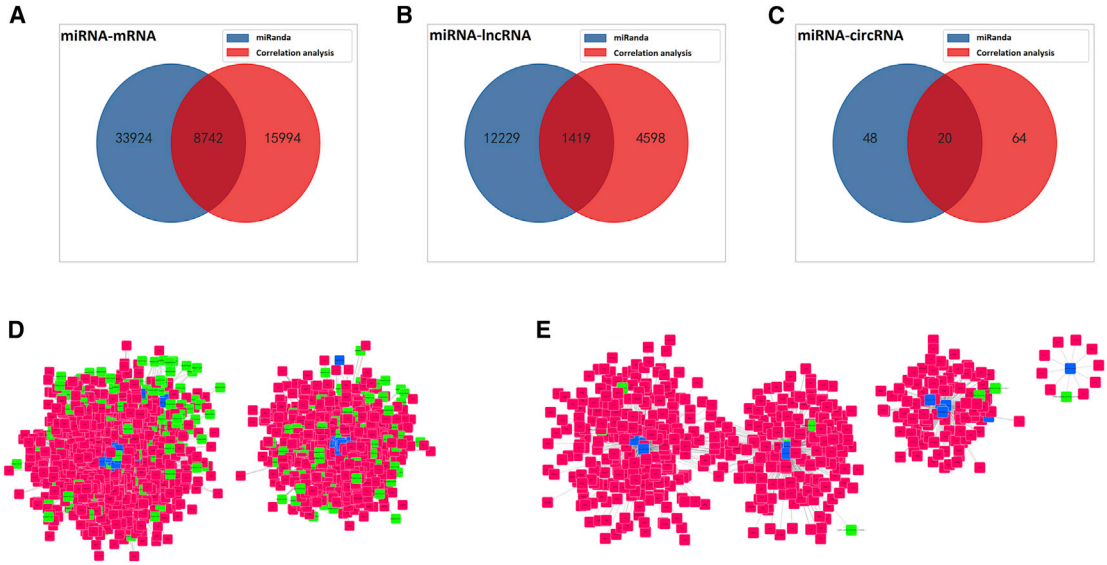

Figure 4. Construction of lncRNA/circRNA-miRNA-mRNA regulatory network among identified DEGs between IR-NOFD and IR groups

(A–C) 8,742 paired miRNA-mRNA (A), 1,419 paired miRNA-lncRNA (B), and 20 paired miRNA-circRNA (C) from the intersections predicted by miRanda and correlation analysis. Parameters for correlation analysis were Pearson's $r > 0.7$ and $p < 0.05$. lncRNA-miRNA-mRNA (D) and circRNA-miRNA-mRNA (E) regulatory networks against predicted miRNA-target gene pairs with shared miRNAs ≥ 5 and $p < 0.05$. lncRNA/circRNA, miRNA, and mRNA are indicated in green, blue, and red, respectively.

demonstrating the successful degradation of linear RNAs. The disappeared of *HPRT* (mRNA) in RNase-R-treated groups also confirmed this result (Figure 7F).

miRNA binding site prediction for lncRNA/circRNA in ceRNA networks

The miRNA binding sites for determined lncRNAs and circRNAs were predicted by RNAhybrid (v.2.2). A miRNA hybridization diagram with minimum free energy (MFE) for each target RNA is displayed in Figure 8. Among them, mmu-miR-92a-1-5p might be a pivotal regulator for all these transcripts, because it was the only miRNA involved in each regulatory network and it possessed the lowest MFE with target RNA (Table S4).

DISCUSSION

Given the relentless renewal ability of intestinal crypt-base stem cells, small intestine in the GI tract is more vulnerable to radiation-induced disruption. However, ideal mitigators in modulating radiation-induced GI toxicity are still deficient. Through PHD inhibitors involving DMOG or FG-4592, the enhancement of HIF stability has been proved to prevent and/or alleviate radiation-induced GI syndrome.[27] Compared to stabilizing the HIF complex, elevating HIF-1α transcriptional activity by selectively blocking its asparaginyl hydroxylase-FIH might be another strategy to exert radioprotection against the GI tract. Previously, we demonstrated that FIH inhibitor-NOFD mitigates cellular ROS levels and reduces cell apoptosis through promoting HIF-1 pathway activity.[28] In this study, we first verified the radioprotective role of FIH inhibitor-NOFD on radiation-induced GI syndrome through observing increased small intestinal integrity, retained crypt stemness, and maintained barrier function of intestinal epithelium. Moreover, we obtained the ceRNA regulatory network of FIH-inhibited groups (by NOFD pre-treatment) and illustrated the therapeutic mechanism of the FIH/HIF axis in IR-induced GI syndrome for the first time.

Through hydroxylating an asparagine residue of HIF-1α, FIH represses its transcriptional activity, resulting in the inhibition of specific gene expression.[29] These genes, including *HK2*, *ADM*, *VEGFA*, *SLC2A1*, and *CDKN1A*, were observed to have upregulated expression in NOFD pre-treated groups, indicating successful de-repression of HIF-1α by NOFD. Accumulated expression of *HK2* and *SLC2A1* also suggests an accelerated glycolytic pathway,[26,30] leading to restrained ROS production in cells. This result is in line with a previous report, wherein activated HIF-1α facilitates anaerobic metabolism and reduces intracellular ROS level by inhibiting its production.[9]

Apart from stimulating the HIF-1 pathway, the radioprotective effect for FIH inhibitor-NOFD also involves the activation of the PI3K-AKT signaling pathway. Their intricate relationship forms a feedback loop: overexpressed HIF-1α in tumor can activate the EGFR/PI3K/AKT pathway, and the activated pathway further induces HIF-1α expression.[31–33] We speculated that the activation of this loop contributes to improving epithelial cell activity by upregulating *EGFR* and accelerating immune cell functions via stimulating inflammatory enzymatic gene *NOS2*,[34,35] resulting in increased radioresistance of the small intestine.

Although the radioprotective effect on normal tissues of HIF-1α has been proved in this study, it might also cause resistance of tumors against chemotherapy or radiotherapy. The role of HIF-1α in tumor progression is controversial. In some tumors HIF-1α appears to drive

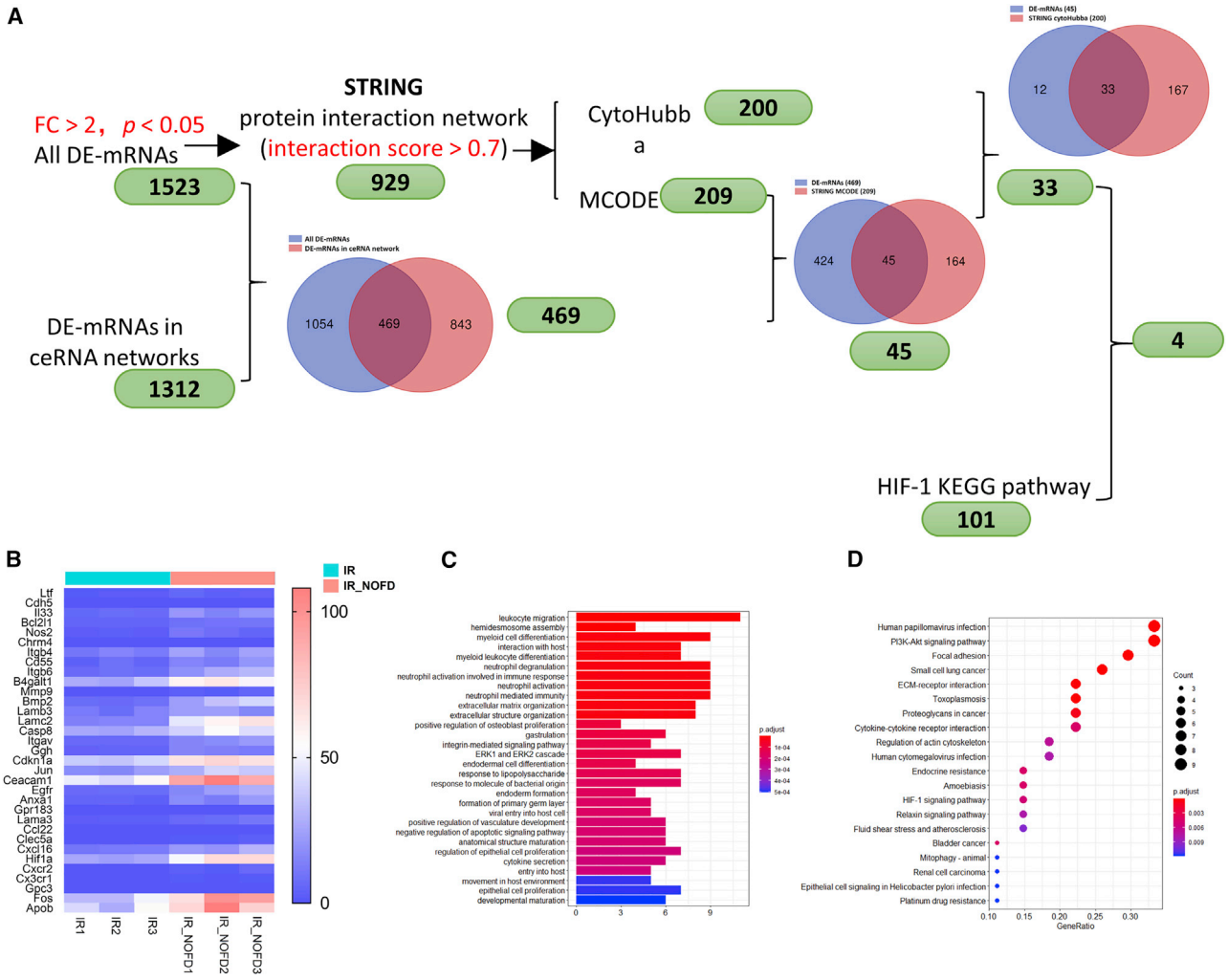

Figure 5. Identification of hub genes in in tremendous dataset between IR-NOFD and IR groups

(A) The workflow of identifying regulatory hub genes. (B) Expression profile of 33 hub genes visualized in heatmap with mRNAs indicated in column and groups represented in row. Top GO functional annotation (C) and KEGG pathway analysis (D) of these hub genes.

tumorigenesis, while in many others, such as kidney cancer, HIF-1α displays as a suppressor.[36,37] Its bidirectional role in tumorigenesis might correlate with a specific tumor microenvironment, including cells of mesenchymal origin, cells of hematopoietic origin, and non-cellular components.[38] Therefore, apart from usage of FIH inhibitor-NOFD in nuclear terrorism as a radioprotector for the GI tract, its application in protecting normal tissues against abdominal or pelvic tumors needs to be precisely determined. GI-tract-targeting therapeutic strategies could be designed to solve this problem.

In addition to activating transcriptional activity of HIF-1α, NOFD can promote its gene expression directly without interfering with FIH stability. This upregulated mechanism was revealed by ceRNA network analysis. In the transcriptional crosstalk, two novel circRNAs (circRNA_2909 and circRNA_0323) and two lncRNAs (NONMMUT140549.1 and NONMMUT148249.1) were identified as vital upstream regulators. Through competitively binding to miRNAs, *HIF1A* and *NOS2* were de-repressed and/or stabilized from shared miRNAs. Among them, mmu-miR-92a-1-5p was the only miRNA shared by each transcript, and its biological role in cardiac regenerative capacity had been demonstrated previously.[39] Therefore, it might be a crucial regulator in the FIH/HIF axis to exert radioprotective activity.

Although the transcriptional crosstalk of the FIH/HIF axis was primarily revealed, the verification of this ceRNA regulatory network is limited in the present study. As crucial regulators in fulfilling biological processes, RNAs can interact with diverse macromolecules, including RNA, DNA, proteins, lipids, and metabolites, to perform intricate functions.[40,41] In addition to the ceRNA regulatory network, other binding molecules such as RNA-binding proteins in RNA-protein interaction might also play important roles in the FIH/HIF axis. Further research needs to be conducted to fully investigate these

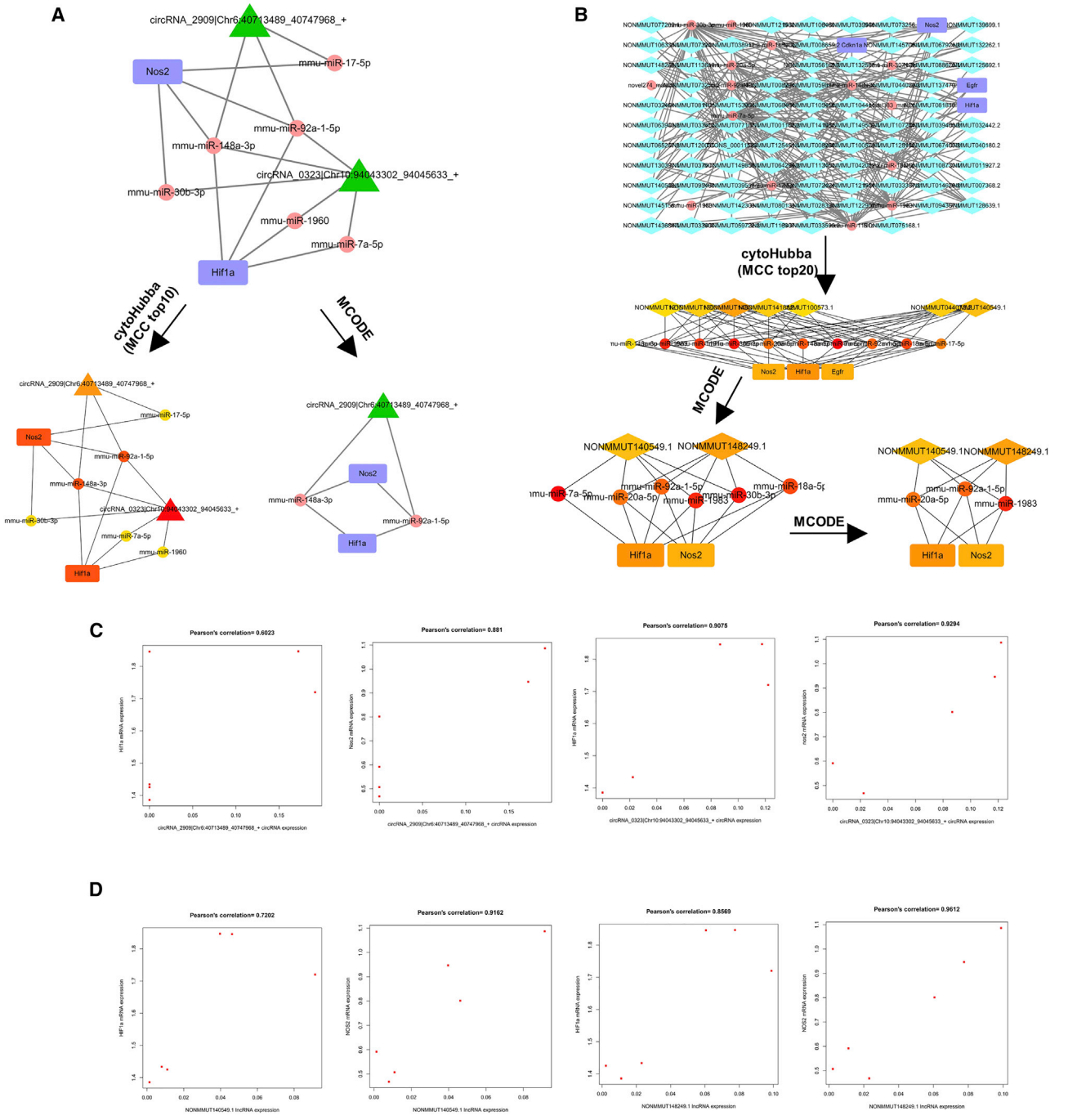

Figure 6. The construction of ceRNA networks against 4 hub genes: *EGFR*, *HIF1A*, *NOS2*, and *CDKN1A*

(A) The workflow for screening *NOS2*- and *HIF1A*-associated circRNA-miRNA-mRNA regulatory network through two plug-ins in Cytoscape software: cytoHubba and MCODE. (B) The workflow for confirming 4 hub gene-associated lncRNA-miRNA-mRNA regulatory networks through cytoHubba and MCODE. circRNAs, lncRNAs, miRNAs, and mRNAs were indicated in triangle, rhombus, circle, and rectangle, respectively. (C) Correlation analyses of circ_2909-*HIF1A*, circ_2909-*NOS2*, circ_0323-*HIF1A*, and circ_0323-*NOS2*. (D) Correlation analyses of NONMMUT140549.1-*HIF1A*, NONMMUT140549.1-*NOS2*, NONMMUT148249.1-*HIF1A*, and NONMMUT148249.1-*NOS2*. Pearson's $r > 0.6$.

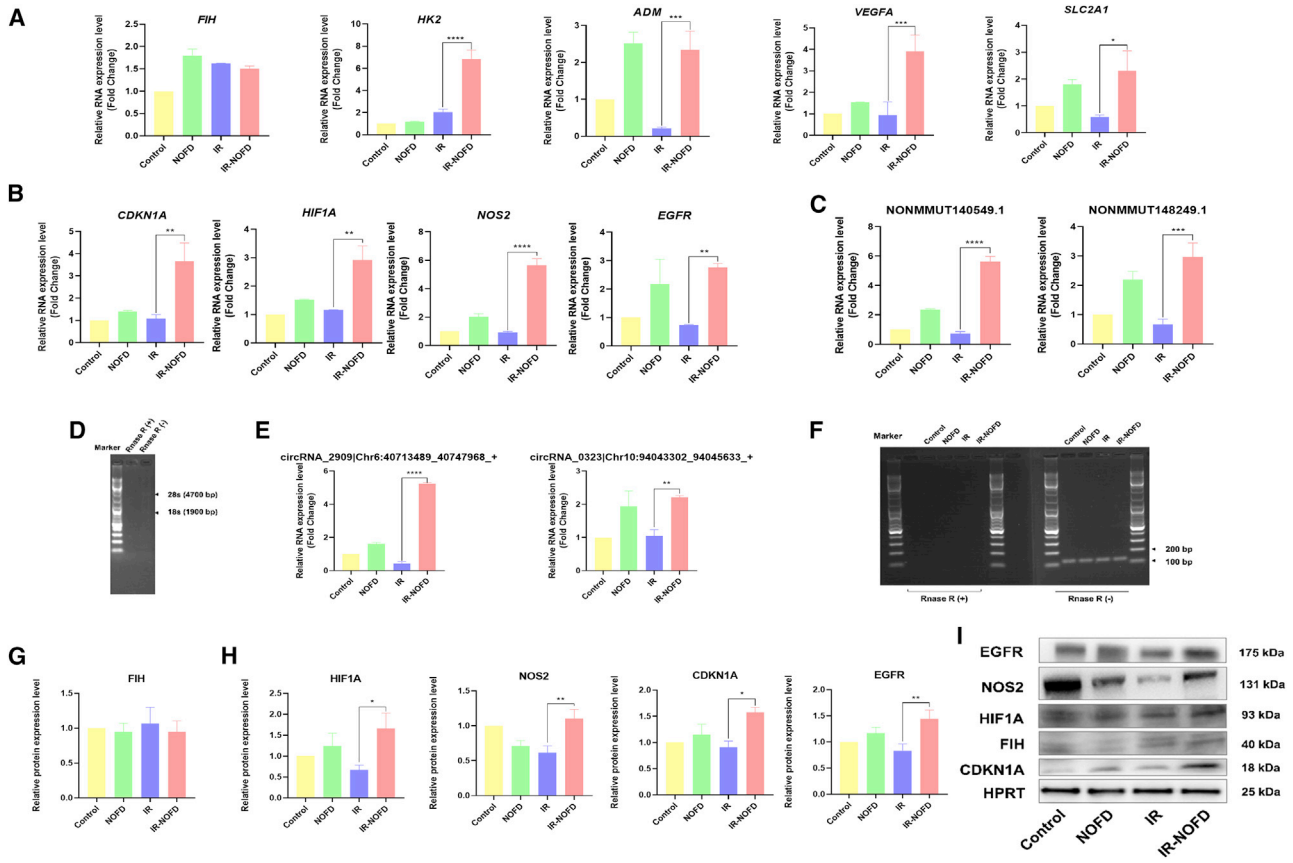

Figure 7. Validation of transcript expressions by quantitative real-time PCR and western blot among control, NOFD, IR, and IR-NOFD groups

(A) The upregulated expression of *HK2*, *ADM*, *VEGFA*, and *SLC2A1* in the IR-NOFD group without interfering FIH protein level, indicating the impeded enzymatic activity of FIH by NOFD. (B and C) The upregulated expressions of the 4 hub genes *HIF1A*, *NOS2*, *EGFR*, and *CDKN1A* (B), and the two lncRNAs, NONMMUT140549.1 and NONMMUT148249.1 (C), in IR-NOFD compared to IR groups by quantitative real-time PCR. (D) The absence of 18S and 28S bands in RNase-R-treated total RNA, indicating the successful degradation of linear RNAs. (E) The upregulated expressions of two circRNAs, circRNA_2909 and circRNA_0323, in IR-NOFD compared to IR groups by quantitative real-time PCR. (F) Validation for degrading linear RNA-HPRT in RNase-R-treated total RNA. (G–I) The upregulated expression of HIF1A, NOS2, EGFR, and CDKN1A in IR-NOFD group compared to IR, without interfering FIH protein level by western blot analysis. A housekeeping gene, *HPRT*, was used as control for normalization in quantitative real-time PCR. *p < 0.05, **p < 0.01, ***p < 0.001, and ****p < 0.0001. Data are reported as mean ± SEM of three independent experiments.

RNAs and their binding partners in regulating radioprotective activities.

Given the occupancy of the FIH-active site pocket by NOFD, this compound blocks asparaginyl hydroxylation of HIF-1α by FIH, resulting in promoted transcriptional activity of the HIF complex.[42] Apart from enhanced HIF-1α function after occupying active site pocket of FIH by NOFD, other substrates for FIH, which relate to nuclear factor-κB (NF-κB) and Notch pathways, might also exert a protective role against IR as their de-repression by NOFD.[43] These substrates share a common motif, ankyrin repeat domain (ARD), leading to efficient hydroxylation of their conserved asparaginyl residue by FIH.[44] However, whether these consensus ARD proteins have a radioprotective effect and how they exert specific functions also need to be addressed in the future.

In total, we verified radioprotection of FIH inhibitor-NOFD in the GI tract and demonstrated that the FIH/HIF axis might be a therapeutic strategy in exploring GI radioprotectors. Furthermore, the ceRNA regulatory network associated with this axis was first illustrated in this study. These data contribute to better understanding of FIH/HIF-associated biological process and lay the foundation for developing radioprotective drugs.

MATERIALS AND METHODS

Synthesis of NOFD

The target compound NOFD was synthesized as reported.[10] All 1H NMR and 13C NMR spectra were recorded on NMR characterization performed on Bruker 300 MHz NMR spectrometers using CDCl3 and DMSO-d6 as the solvent.

Animals

Male C57BL/6 mice (6–8 weeks) were purchased from Beijing Vital River Laboratory Animal Technology (Beijing, China) and acclimated to the environment (specific-pathogen-free, 22°C ± 2°C, 50%

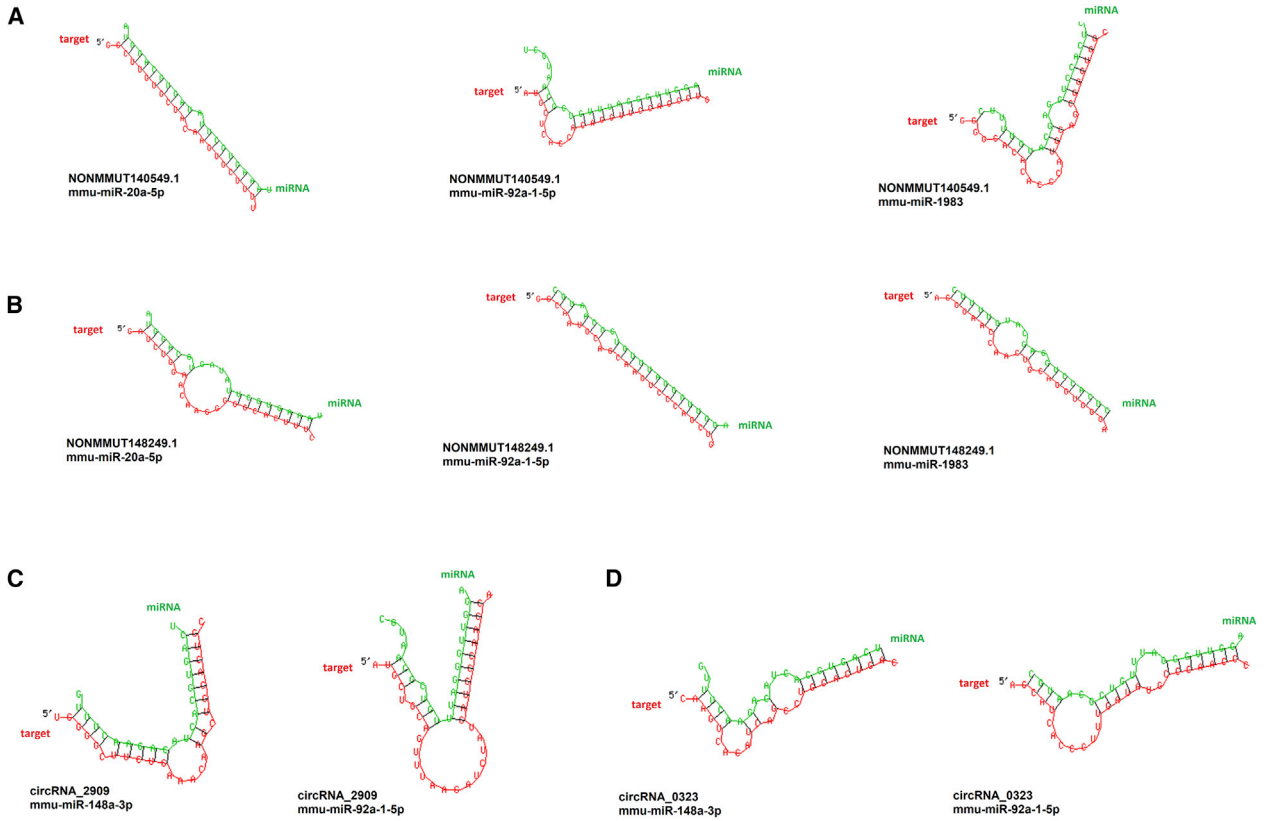

Figure 8. Predicted miRNA binding sites for determining lncRNA/circRNA via RNAhybrid

(A) Binding sites for NONMMUT140549.1 with three different miRNAs including mmu-miR-20a-5p, mmu-miR-92a-1-5p, and mmu-miR-1983. (B) Binding sites for NONMMUT148249.1 with three different miRNAs. (C) Binding sites for circRNA_2909 with two different miRNAs involving mmu-miR-148a-3p and mmu-miR-92a-1-5p. (D) Predicted binding sites among circRNA_0323 and two miRNAs, mmu-miR-148a-3p and mmu-miR-92a-1-5p.

humidity, and 12 h light/dark cycle) for 7 days with free access to standard diet. Mice were intraperitoneally injected with 0.2 mL, 5 mg/kg NOFD or 0.9% isotonic saline (control group) at indicated time points (Figure 1B). After being anesthetized and fixed on a steel chamber, they were abdominally irradiated with a single dose of 13 Gy γ-ray by using a Gammacell 40 Exactor (Atomic Energy of Canada, Chalk River, Ottawa, ON, Canada) at a rate of 1 Gy/min. All animal experiments were conducted with the guidance of the local animal care and use committee.

Histology

After receiving 13 Gy ABI for 3.5 days, the small intestines were collected and stained with hematoxylin and eosin (H&E). In order to carry out morphological analysis (including the villi length and crypts) for small intestine, ImageJ 1.37 software was used to blindly analyze six circular cross-sections from the coded H&E staining digital photographs.

Immunohistochemical analysis

The paraffin-embedded sections of small intestine were incubated with anti-Ki67 (1:300 dilution; Novus, Littleton, CO, USA), anti-Lgr5 (1:50 dilution; Abcam, Cambridge, MA, USA), and anti-villi (1:800 dilution; Abcam) in a wet box at 4°C overnight. After incubated for 1 h in secondary antibody for 30 min at 37°C, the sections were captured by a microscope. Positive cells were detected by DAB kit (Sigma-Aldrich, St. Louis, MO, USA). Performance primitive (IPP) software was adopted to objectively capture the image and quantify the positive staining among these sections.

Terminal deoxynucleotidyl transferase dUTP nick-end labeling assay

Apoptosis in the intestinal tissue was determined by an *in situ* Cell Death Detection Kit (Roche Diagnostic, Mannheim, Germany) according to the manufacturer's protocol and analyzed under a laser confocal scanning microscope.

Immunofluorescence analysis

As mentioned above, after the paraffin-embedded sections of the small intestine were repaired with antigens and blocked, the sections incubated with anti-caspase-8 (1 caspase-8 100 diluted; CST, Danvers, MA, USA), anti-caspase-9 (1 caspase-9 1,000 diluted; CST) at 4°C. Then the sections were incubated in the second antibody at

37°C after washing with PBS. Finally, the sections were sealed with a sealant containing 4-methylidene 6-di-mid-2-phenyl indole. The image was captured by laser scanning confocal microscope.

Intestinal permeability assay

After 13 Gy ABI for 3.5 days, the mice were fasted for 12 h and gavaged with 0.6 mg/g body weight of a FITC-dextran solution (4 kDa, Sigma-Aldrich, Spain) for 4 h prior to sacrifice. Blood was taken by cardiac puncture and serum was obtained by centrifugation at 1,000 rpm for 15 min. Fluorescence intensity of each serum sample (DTX 880 Multimode Detector, USA) was measured.

Cell preparation and RNA-seq

At 3.5 days post-radiation, all mice were sacrificed, and their small intestines were harvested for extracting crypts. The isolation procedures followed those of O'Rourke et al.[45] Total RNA was extracted from isolated crypts in each group using RNAeasy Plus Animal RNA Isolation Kit with Spin Column (Beyotime Institute of Biotechnology, China). RNA integrity was evaluated on Agilent 2100 Bioanalyzer (Agilent Technologies, Santa Clara, CA, USA) with RNA integrity number (RIN) $\geq$ 7 conserved for subsequent analysis. Subsequently, using TruSeq Stranded Total RNA with Ribo-Zero Gold (Illumina, San Diego, CA, USA), RNA libraries were prepared and sequenced on the Illumina sequencing platform (HiSeq 2500).

Sequence assembling

The RNA-seq fastq raw reads were first filtered using Trimmomatic software to remove low-quality reads. Furthermore, screened clean reads could align to the mouse reference genome to obtain different transcripts followed by hisat2. Apart from known transcripts, other new sequences were spliced using Stringtie software. lncRNA transcripts were constructed using Cuffcompare software followed by CPC, CNCI, Pfam, and PLEK to screen out coding potential sequences of predicted lncRNAs, while circRNA sequences were predicted based on junction reads and GT-AG cleavage signals using CIRI software. (Gene sequences were uploaded as SRA accession number SRA: PRJNA728840.)

Differential expression analysis

Differentially expressed transcripts between NOFD (named as IR_-NOFD) or 0.9% isotonic saline (named as IR) treatment groups on the radiation-induced intestinal mouse model were performed using the DESeq R package (2012). Through the nbinomTest function, all selected transcripts with p values $\leq$ 0.05 and $|(\text{fold change})| \geq 2$ were finally considered as significantly differentially expressed.

ceRNA network construction

Due to the common MREs, lncRNAs, circRNAs, and mRNAs in the cytoplasm can compete in binding to miRNAs and influence each other's expression. Thereby, to visualize their interaction network, circRNA/lncRNA-miRNA interactions were predicted using miRanda software, while target genes for those predicted miRNAs were identified through Targetscan.

Hub gene identification

STRING 11.0 (https://string-db.org/) was used to construct a PPI network among all DEGs. After visualizing this result in Cytoscape (v.3.6.0) software, two plug-ins (MCODE and CytoHubba) were used to identify hub genes in this redundant network through calculating correlation levels and the highest linkage among those nodes respectively.

GO, KEGG, and correlation analyses

GO and KEGG pathway analyses of screened genes were performed by clusterProfiler R package (v.3.18.0). Pearson correlation coefficients of identified hub genes in the ceRNA network were also analyzed through the R package.

Quantitative real-time PCR validation

Total RNA was isolated using RNAeasy Plus Animal RNA Isolation Kit with Spin Column (Beyotime Institute of Biotechnology, China). PrimeScript RT reagent Kit (Perfect Real Time) (Takara, Japan) was used to perform reverse transcription of lncRNA and mRNA. After cDNA was synthesized, quantitative real-time PCR reactions were conducted on a Bio-Rad CFX96 Real-Time Detection System using BlasTaq 2X qPCR MasterMix (Applied Biological Materials, Canada).

To evaluate the expression of circRNA, total RNA was first incubated with RNase R (Epicenter, 40 U, 37°C, 3 h) to degrade straight-chain RNA, followed by 70°C, 10 min for enzyme inactivation. Subsequently, cDNA was synthesized and circRNA expression was monitored by quantitative real-time PCR . Primer pairs are presented in Table S5.

Binding site prediction for miRNA sponges

Predicted binding sites between lncRNA/circRNA and miRNA were performed by RNAhybrid tool (https://bibiserv.cebitec.uni-bielefeld.de/rnahybrid). Through calculating the minimum free energy hybridization among those RNAs, RNAhybrid can exhibit the best predicted fitting part.

Western blot analysis

After isolation of crypts in C57BL/6 mice, total proteins were extracted from those cells using RIPA lysis buffer (1% PMSF) (Solarbio Science & Technology, China). The primary antibodies included anti-EGFR (1:1,000; catalog no. Ab52894, Abcam, UK), anti-NOS2 (1:1,000; catalog no. Ab178945, Abcam, UK), anti-HIF-1α (1:500; catalog no. Ab179483, Abcam, UK), anti-FIH (1:1,000; catalog no. Ab178945, Abcam, UK), anti-Cdkn1a (1:1,000; catalog no. Ab188224, Abcam, UK), and anti-HPRT (1:10,000; catalog no. Ab109021, Abcam, UK). Goat anti-rabbit immunoglobulin G (IgG)-horseradish peroxidase (HRP) (1:10,000; catalog no. BS13278, Bioworld Technology) was used as a secondary antibody.

Statistical analysis

All statistical analyses were performed using GraphPad Prism 8.0 (GraphPad Software, San Diego, CA, USA). Data are reported as mean ± SEM of three independent experiments. Multiple-group

comparisons were performed by one-way ANOVA. Significant difference was considered when p value < 0.05, as indicated in figure legends.

SUPPLEMENTAL INFORMATION

Supplemental information can be found online at https://doi.org/10.1016/j.omtn.2021.05.008.

ACKNOWLEDGMENTS

This work was supported by CAMS Innovation Fund for Medical Sciences (CIFMS, 2017-I2M-3-019).

AUTHOR CONTRIBUTIONS

Conceptualization, Y.Y., X.M., Y.M., and W.X.; investigation and methodology, Y.Y., X.M., Y.M., H.T., M.C., and Z.Z.; visualization, Y.Y., X.M., and Y.M.; Resources, W.X., and W.L.; writing – original draft, Y.Y., X.M., and Y.M.; writing – review & editing, Y.Y., X.M., and W.X.; Supervision, W.X.; funding acquisition, W.X., and W.L.

DECLARATION OF INTERESTS

The authors declare no competing interests.

REFERENCES

1. de la Cruz Bonilla, M., Stemler, K.M., Taniguchi, C.M., and Piwnica-Worms, H. (2018). Stem cell enriched-epithelial spheroid cultures for rapidly assaying small intestinal radioprotectors and radiosensitizers in vitro. Sci. Rep. *8*, 15410.
2. Confer, D., Chao, N., and Case, C., Jr. (2018). Are We Prepared for Nuclear Terrorism? N. Engl. J. Med. *378*, 2447.
3. Rezvani, M. (2021). Therapeutic Potential of Mesenchymal Stromal Cells and Extracellular Vesicles in the Treatment of Radiation Lesions-A Review. Cells *10*, 427.
4. Clayton, N.P., Khan-Malek, R.C., Dangler, C.A., Zhang, D., Ascah, A., Gains, M., Gardner, B., Mockbee, C., Keutzer, J.M., McManus, J., and Authier, S. (2021). Sargramostim (rhu GM-CSF) Improves Survival of Non-Human Primates with Severe Bone Marrow Suppression after Acute, High-Dose, Whole-Body Irradiation. Radiat. Res. *195*, 191–199.
5. Aaseth, J., Nurchi, V.M., and Andersen, O. (2019). Medical Therapy of Patients Contaminated with Radioactive Cesium or Iodine. Biomolecules *9*, 856.
6. Robinson, A., Keely, S., Karhausen, J., Gerich, M.E., Furuta, G.T., and Colgan, S.P. (2008). Mucosal protection by hypoxia-inducible factor prolyl hydroxylase inhibition. Gastroenterology *134*, 145–155.
7. Krock, B.L., Skuli, N., and Simon, M.C. (2011). Hypoxia-induced angiogenesis: good and evil. Genes Cancer *2*, 1117–1133.
8. Olcina, M.M., and Giaccia, A.J. (2016). Reducing radiation-induced gastrointestinal toxicity - the role of the PHD/HIF axis. J. Clin. Invest. *126*, 3708–3715.
9. Sun, R., Meng, X., Pu, Y., Sun, F., Man, Z., Zhang, J., Yin, L., and Pu, Y. (2019). Overexpression of HIF-1a could partially protect K562 cells from 1,4-benzoquinone induced toxicity by inhibiting ROS, apoptosis and enhancing glycolysis. Toxicol. In Vitro *55*, 18–23.
10. Meng, Y., Yang, F., Long, W., and Xu, W. (2018). Radioprotective Activity and Preliminary Mechanisms of *N*-oxalyl-d-phenylalanine (NOFD) In Vitro. Int. J. Mol. Sci. *20*, 37.
11. Wang, G.L., and Semenza, G.L. (1993). Characterization of hypoxia-inducible factor 1 and regulation of DNA binding activity by hypoxia. J. Biol. Chem. *268*, 21513–21518.
12. Mahon, P.C., Hirota, K., and Semenza, G.L. (2001). FIH-1: a novel protein that interacts with HIF-1alpha and VHL to mediate repression of HIF-1 transcriptional activity. Genes Dev. *15*, 2675–2686.
13. Kang, J., Chun, Y.S., Huh, J., and Park, J.W. (2018). FIH permits NAA10 to catalyze the oxygen-dependent lysyl-acetylation of HIF-1α. Redox Biol. *19*, 364–374.
14. Kim, I., Shin, S.H., Lee, J.E., and Park, J.W. (2019). Oxygen sensor FIH inhibits HACE1-dependent ubiquitination of Rac1 to enhance metastatic potential in breast cancer cells. Oncogene *38*, 3651–3666.
15. Fraisl, P., Aragonés, J., and Carmeliet, P. (2009). Inhibition of oxygen sensors as a therapeutic strategy for ischaemic and inflammatory disease. Nat. Rev. Drug Discov. *8*, 139–152.
16. Eltzschig, H.K., Bratton, D.L., and Colgan, S.P. (2014). Targeting hypoxia signalling for the treatment of ischaemic and inflammatory diseases. Nat. Rev. Drug Discov. *13*, 852–869.
17. Sim, J., Cowburn, A.S., Palazon, A., Madhu, B., Tyrakis, P.A., Macías, D., Bargiela, D.M., Pietsch, S., Gralla, M., Evans, C.E., et al. (2018). The Factor Inhibiting HIF Asparaginyl Hydroxylase Regulates Oxidative Metabolism and Accelerates Metabolic Adaptation to Hypoxia. Cell Metab. *27*, 898–913.e7.
18. Zhang, P., Du, J., Zhao, H., Cheng, Y., Dong, S., Yang, Y., Li, B., Gao, F., Sun, X., Cai, J., and Liu, C. (2019). Radioprotective effects of roxadustat (FG-4592) in haematopoietic system. J. Cell. Mol. Med. *23*, 349–356.
19. Salmena, L., Poliseno, L., Tay, Y., Kats, L., and Pandolfi, P.P. (2011). A ceRNA hypothesis: The Rosetta Stone of a hidden RNA language? Cell *146*, 353–358.
20. Tay, Y., Rinn, J., and Pandolfi, P.P. (2014). The multilayered complexity of ceRNA crosstalk and competition. Nature *505*, 344–352.
21. Fernandez Vallone, V., Leprovots, M., Ribatallada-Soriano, D., Gerbier, R., Lefort, A., Libert, F., Vassart, G., and Garcia, M.I. (2020). LGR5 controls extracellular matrix production by stem cells in the developing intestine. EMBO Rep. *21*, e49224.
22. Hauer-Jensen, M., Denham, J.W., and Andreyev, H.J. (2014). Radiation enteropathy–pathogenesis, treatment and prevention. Nat. Rev. Gastroenterol. Hepatol. *11*, 470–479.
23. Enright, A.J., John, B., Gaul, U., Tuschl, T., Sander, C., and Marks, D.S. (2003). MicroRNA targets in Drosophila. Genome Biol. *5*, R1.
24. Liu, Y., Gu, H.Y., Zhu, J., Niu, Y.M., Zhang, C., and Guo, G.L. (2019). Identification of Hub Genes and Key Pathways Associated With Bipolar Disorder Based on Weighted Gene Co-expression Network Analysis. Front. Physiol. *10*, 1081.
25. McDonough, M.A., McNeill, L.A., Tilliet, M., Papamicaël, C.A., Chen, Q.Y., Banerji, B., Hewitson, K.S., and Schofield, C.J. (2005). Selective inhibition of factor inhibiting hypoxia-inducible factor. J. Am. Chem. Soc. *127*, 7680–7681.
26. Ramos, H., Calheiros, J., Almeida, J., Barcherini, V., Santos, S., Carvalho, A.T.P., Santos, M.M.M., and Saraiva, L. (2020). SLMP53-1 Inhibits Tumor Cell Growth through Regulation of Glucose Metabolism and Angiogenesis in a P53-Dependent Manner. Int. J. Mol. Sci. *21*, 596.
27. Fujimoto, T.N., Colbert, L.E., Huang, Y., Molkentine, J.M., Deorukhkar, A., Baseler, L., de la Cruz Bonilla, M., Yu, M., Lin, D., Gupta, S., et al. (2019). Selective EGLN Inhibition Enables Ablative Radiotherapy and Improves Survival in Unresectable Pancreatic Cancer. Cancer Res. *79*, 2327–2338.
28. Taylor, C.T., and Colgan, S.P. (2017). Regulation of immunity and inflammation by hypoxia in immunological niches. Nat. Rev. Immunol. *17*, 774–785.
29. Dayan, F., Roux, D., Brahimi-Horn, M.C., Pouyssegur, J., and Mazure, N.M. (2006). The oxygen sensor factor-inhibiting hypoxia-inducible factor-1 controls expression of distinct genes through the bifunctional transcriptional character of hypoxia-inducible factor-1alpha. Cancer Res. *66*, 3688–3698.
30. Petrasca, A., Phelan, J.J., Ansboro, S., Veale, D.J., Fearon, U., and Fletcher, J.M. (2020). Targeting bioenergetics prevents CD4 T cell-mediated activation of synovial fibroblasts in rheumatoid arthritis. Rheumatology (Oxford) *59*, 2816–2828.
31. Lee, S.Y., Jeong, E.K., Ju, M.K., Jeon, H.M., Kim, M.Y., Kim, C.H., Park, H.G., Han, S.I., and Kang, H.S. (2017). Induction of metastasis, cancer stem cell phenotype, and oncogenic metabolism in cancer cells by ionizing radiation. Mol. Cancer *16*, 10.
32. Zhang, H.X., Yang, J.J., Zhang, S.A., Zhang, S.M., Wang, J.X., Xu, Z.Y., and Lin, R.Y. (2018). HIF-1α promotes inflammatory response of chronic obstructive pulmonary disease by activating EGFR/PI3K/AKT pathway. Eur. Rev. Med. Pharmacol. Sci. *22*, 6077–6084.
33. Gao, T., Zhang, X., Zhao, J., Zhou, F., Wang, Y., Zhao, Z., Xing, J., Chen, B., Li, J., and Liu, S. (2020). SIK2 promotes reprogramming of glucose metabolism through PI3K/

AKT/HIF-1α pathway and Drp1-mediated mitochondrial fission in ovarian cancer. Cancer Lett. *469*, 89–101.

34. Jantsch, J., Wiese, M., Schödel, J., Castiglione, K., Gläsner, J., Kolbe, S., Mole, D., Schleicher, U., Eckardt, K.U., Hensel, M., et al. (2011). Toll-like receptor activation and hypoxia use distinct signaling pathways to stabilize hypoxia-inducible factor 1α (HIF1A) and result in differential HIF1A-dependent gene expression. J. Leukoc. Biol. *90*, 551–562.

35. Rodrigues, T.S., Alvarez, A.R.P., Gembre, A.F., Forni, M.F.P.A.D., de Melo, B.M.S., Alves Filho, J.C.F., Câmara, N.O.S., and Bonato, V.L.D. (2020). Mycobacterium tuberculosis-infected alveolar epithelial cells modulate dendritic cell function through the HIF-1α-NOS2 axis. J. Leukoc. Biol. *108*, 1225–1238.

36. Wang, X., Li, L., Zhao, K., Lin, Q., Li, H., Xue, X., Ge, W., He, H., Liu, D., Xie, H., et al. (2020). A novel LncRNA HITT forms a regulatory loop with HIF-1α to modulate angiogenesis and tumor growth. Cell Death Differ. *27*, 1431–1446.

37. Shen, C., Beroukhim, R., Schumacher, S.E., Zhou, J., Chang, M., Signoretti, S., and Kaelin, W.G., Jr. (2011). Genetic and functional studies implicate HIF1α as a 14q kidney cancer suppressor gene. Cancer Discov. *1*, 222–235.

38. Huang, Y., Lin, D., and Taniguchi, C.M. (2017). Hypoxia inducible factor (HIF) in the tumor microenvironment: friend or foe? Sci. China Life Sci. *60*, 1114–1124.

39. Liu, H.L., Zhu, J.G., Liu, Y.Q., Fan, Z.G., Zhu, C., and Qian, L.M. (2014). Identification of the microRNA expression profile in the regenerative neonatal mouse heart by deep sequencing. Cell Biochem. Biophys. *70*, 635–642.

40. Dai, X., Zhang, S., and Zaleta-Rivera, K. (2020). RNA: interactions drive functionalities. Mol. Biol. Rep. *47*, 1413–1434.

41. Nechay, M., and Kleiner, R.E. (2020). High-throughput approaches to profile RNA-protein interactions. Curr. Opin. Chem. Biol. *54*, 37–44.

42. Conejo-Garcia, A., McDonough, M.A., Loenarz, C., McNeill, L.A., Hewitson, K.S., Ge, W., Liénard, B.M., Schofield, C.J., and Clifton, I.J. (2010). Structural basis for binding of cyclic 2-oxoglutarate analogues to factor-inhibiting hypoxia-inducible factor. Bioorg. Med. Chem. Lett. *20*, 6125–6128.

43. Tiwari, V., Kamran, M.Z., Ranjan, A., Nimesh, H., Singh, M., and Tandon, V. (2017). Akt1/NFκB signaling pathway activation by a small molecule DMA confers radioprotection to intestinal epithelium in xenograft model. Free Radic. Biol. Med. *108*, 564–574.

44. Cockman, M.E., Webb, J.D., and Ratcliffe, P.J. (2009). FIH-dependent asparaginyl hydroxylation of ankyrin repeat domain-containing proteins. Ann. N Y Acad. Sci. *1177*, 9–18.

45. O'Rourke, K.P., Ackerman, S., Dow, L.E., and Lowe, S.W. (2016). Isolation, Culture, and Maintenance of Mouse Intestinal Stem Cells. Bio Protoc. *6*, e1733.